



Elucidating the mechanism of the reverse water–gas shift reaction over Au/CeO₂ catalysts using *operando* and transient spectroscopies

Marc Ziemba¹, Jakob Weyel¹, Christian Hess^{*}

Eduard-Zintl-Institute of Inorganic and Physical Chemistry, Technical University of Darmstadt, Alarich-Weiss-Str. 8, 64287 Darmstadt, Germany

ARTICLE INFO

Keywords:

Gold-based catalyst
CeO₂
Reverse water–gas shift
CO₂ activation
Operando spectroscopy

ABSTRACT

The reaction mechanism of the reverse water–gas shift reaction (rWGS) over Au/ceria catalysts was investigated by monitoring the catalyst dynamics and reaction intermediates using *operando* and transient spectroscopies, as well as by DFT calculations. Combined *operando* Raman and UV-Vis spectroscopic analysis allows establishing a correlation between subsurface oxygen vacancies and catalytic activity. Comparison of different ceria support materials, i.e., polyhedra and polycrystalline sheets, reveals that the defect concentration is not rate-determinant. Using transient DRIFTS, we are able to identify individual steps of hydrogen dissociation on supported gold and to gain detailed insight into the reduction of CO₂ via formate and carbonate formation. It is demonstrated that CO₂ reduction is influenced by the surface pretreatment. Considering all spectroscopic findings, we propose an associative mechanism via carbonate and formate intermediates as the main route for the rWGS over Au/ceria(111) catalysts, while a redox mechanism plays only a minor role.

1. Introduction

The ever-increasing levels of CO₂ emissions [1] and the resulting impact of the greenhouse effect are the main reasons for the importance of dealing with CO₂, while solutions to stop its further release into the atmosphere continue to be sought after. In an increasing number of CO₂ capture technologies, its activation and use as a C1 source is an attractive strategy [2]. It is of particular interest to use CO₂ as a non-fossil source for the production of syngas, owing to its versatility and relevance for a multitude of applications. In this context the reverse water–gas shift reaction (rWGS) plays an important role in the energy sector, allowing CO₂ to be converted first to CO and then to liquid fuels via CO hydrogenation (Fischer–Tropsch process).

While noble metal-loaded CeO₂ catalysts have been shown to be active for the rWGS [3,4], their mode of operation (redox vs associative mechanism) is still a matter of debate. For example, previous studies on Pt/CeO₂ catalysts have shown that intermediates such as carbonates or formates play an important role in the reaction, pointing to an associative mechanism [5,6]. In contrast, the water–gas shift reaction at 300 °C proceeds largely via a redox mechanism [7]. Considerable catalytic activity as well as the appearance of intermediates such as formates or bidentate carbonates was also reported for Cu/CeO₂ catalysts

[8]. In this context, a facet dependence of the ceria support was reported, with the CeO₂(110) surface showing a much higher activity than the CeO₂(111) surface [8]. In contrast, experiments on the bare supports, which become active at temperatures >550 °C [9], have shown that the effect of the surface termination is much smaller [9], highlighting the importance of the metal–support interaction.

Regarding other supports, recent *operando* studies of the rWGS over gold-loaded catalysts, comparing a redox active (Au/TiO₂) with an inactive (Au/Al₂O₃) support, are of interest in the context of the present study [10]. In particular, the reaction over Au/Al₂O₃ is shown to occur via intermediates such as formates, while for the Au/TiO₂ catalyst a redox mechanism involving the formation of hydroxycarbonyls has been postulated, following earlier studies on copper- and gold-loaded TiO₂(110) catalysts during the water–gas shift reaction [11]. With increasing temperature, the associative mechanism is found to contribute more strongly, due to more facile decomposition of adsorbates such as carbonates and formates, thereby releasing CO [10].

This study will focus on Au/CeO₂ catalysts that are known to be active for the rWGS [12,13] and water–gas shift reaction (WGS) [14–17]. While previous studies have demonstrated that Au/CeO₂ catalysts [12] as well as bare ceria [18,19] can be re-oxidized by CO₂, indicating a redox mechanism, the role of adsorbates/reaction

^{*} Corresponding author.

E-mail address: christian.hess@tu-darmstadt.de (C. Hess).

¹ These authors contributed equally.

intermediates has not been clarified yet. In this context, it is of particular interest to explore the role of gold during the re-oxidation process and its contribution during rWGS. For LT-WGS and CO oxidation it has previously been shown that the gold/ceria interface and size distribution have an influence on the catalytic activity [20,21]. Using XAS and DRIFTS during LT-WGS gold was found to be metallic [22], but under reductive conditions or in long-term studies agglomeration of surface gold atoms to small gold particles can occur [23]. Applying *operando* SSITKA-mass spectrometry-DRIFTS to the LT-WGS over a 0.5 wt% Pt/Ce_{1-x}La_xO_{2-δ} catalyst has revealed that the active species is not only formed on the Pt particle but also in its environment [24], which again underlines the importance of the metal-support interaction. In addition, previous studies have shown that hydrogen dissociation on stoichiometric ceria, which leads to the formation of two surface hydroxides, requires temperatures > 400 °C [25]. However, surface oxygen defects significantly affect the H₂ adsorption, giving rise to increased heterolytic dissociation (Ce-H and OH) [25,26]. On Au/CeO₂ catalysts, heterolytic dissociation is feasible at 150 °C, leading to a hydroxide and a gold hydride species [27]. Furthermore, studies on different gold supported materials have shown that an increase in the gold loading results in a higher surface hydroxide concentration, thus providing direct evidence for a gold-catalyzed H₂ dissociation [28].

To elucidate the rWGS reaction mechanism in detail, we employed combined *operando* Raman and UV-Vis as well as transient DRIFTS measurements, supplemented by quasi *in situ* XPS, enabling us to address the support and (transient) adsorbate dynamics, as well as the surface state of Au/CeO₂ catalysts, in an integrated manner. We obtain insight into the role of the support by using ceria with two different particle shapes, i.e., polycrystalline ceria and ceria polyhedra. While polyhedra terminate exclusively with the CeO₂(111) surface, the polycrystalline ceria, which resembles sheets, also contains stepped sites. Previous studies have shown a positive effect of stepped sites on the activity during CO oxidation over Au/CeO₂ catalysts [29].

2. Experimental section

2.1. Catalyst preparation

Polycrystalline ceria sheets were prepared by decomposition of cerium nitrate as described in previous studies [15,30]. Briefly, Ce(NO₃)₃·6H₂O (Alfa Aesar, 99.5%) was calcined at 600 °C (6 °C/min) for 12 h. After cooling to room temperature, the powder was sieved (200 μm) and calcined again using the same protocol. Ceria polyhedra were obtained commercially (Sigma Aldrich, <25 nm (BET)). Gold was loaded onto ceria by electrolyte deposition using a 10⁻³ M HAuCl₄·3H₂O solution (Carl Roth, 99.9%), as described in detail elsewhere [15,30].

2.2. Catalyst characterization

2.2.1. Operando spectroscopy

Combined *operando* Raman and UV-Vis spectra as well as the catalytic activity were measured with a previously described experimental setup [14,15,31,32]. Briefly, for the *operando* measurements, about 20–25 mg of the sample was placed in a stainless steel sample holder (8 mm diameter, 0.5 mm depth). Due to the cell geometry and as the catalyst sample is overflowed by the gases, the amount of catalyst has hardly any influence on the activity. The sample temperature was determined by means of a Ni/Cr-Ni thermocouple (type K), which was located at the sample holder close to the catalyst. Measured temperatures deviated by a maximum of 3 °C from the set temperatures in a constant gas stream. The catalyst temperature was set to 250 °C in all measurements. Raman spectra were recorded with an HL5R transmission spectrometer (Kaiser Optical), using a frequency-doubled Nd:YAG laser (Cobolt) for excitation at 532 nm. The laser power at the position of the sample was 1 mW, as measured with a power meter (Ophir). The spectral resolution was specified as 5 cm⁻¹ and the band

position stability was better than 0.3 cm⁻¹. Spectra of the gold-loaded catalysts were recorded with an exposure time of 225 s and 2 accumulations and those of the bare samples with an exposure time of 150 s and 3 accumulations. For all measurements a cosmic ray filter and an auto new dark correction were applied, resulting in a total measuring time of about 1800 s for the bare and gold-loaded samples. All Raman spectra reported in this work were normalized to the band with the highest intensity, i.e., the F_{2g} band. The given F_{2g} positions were determined by curve fitting using Lorentzian functions.

UV-Vis spectra were recorded in diffuse reflection using an AvaSpec ULS2048 spectrometer (Avantes) equipped with a deuterium lamp and a halogen discharge lamp. Spectra were taken before and after a Raman spectrum. The total measuring time was 60 s, resulting from 200 runs with an exposure time of 300 ms each. As white standard, magnesium oxide powder (Sigma Aldrich) was employed, which shows no absorption within 170–1100 nm.

The gases CO₂ (99.999%, Westfalen), H₂ (99.999%, Westfalen), and argon (99.996%, Westfalen) were dosed by digital mass flow controllers (MFCs, Bronkhorst). Gas atmospheres of 10 vol% H₂/Ar, 2 vol% CO₂/Ar, and 4 vol% H₂/2 vol% CO₂/Ar for reactive conditions were applied at a total flow rate of 100 mL/min. All gas compositions are balanced in argon to keep the turnover low and to eliminate the influence of possible transport effects thus allowing to focus on the reaction mechanism. To analyze the gas phase and its composition, a Fourier transform infrared (FTIR) spectrometer (Tensor 20, Bruker) was installed at the outlet of the reaction cell. The resolution was 4 cm⁻¹, and the measurement time was 1 min, in which 125 spectra were accumulated. Using calibration curves, the concentration of CO was calculated, allowing the conversion of CO₂ to CO to be determined. The catalytic activity is the ratio of the amount of CO, as measured by FTIR at the outlet of the cell, to the amount of dosed CO₂. The activity of the empty cell, which showed a CO₂ conversion of 4.2%, was taken into account when calculating the catalyst activities given in the following. Please note that this background activity is a result of the cell specifications and has been shown to be reproducible.

2.2.2. Transient DRIFTS

Diffuse reflectance IR Fourier transform spectroscopy (DRIFTS) was performed on a Vertex 70 (Bruker) FTIR spectrometer equipped with a liquid nitrogen cooled mercury cadmium telluride (MCT) detector and a commercial reaction cell (Praying Mantis™ High Temperature Reaction Chamber, Harrick Scientific Products) with infrared transparent KBr windows, as described previously [30,33].

As background, the catalyst itself was employed after a 15-minute exposure at 250 °C to H₂ (4 mol%) or CO₂ (2 mol%) or the reaction mixture (4 mol% H₂ and 2 mol% CO₂, balanced with argon; total gas flow: 100 mL/min). For transient measurements we employed the rapid scan mode extension of Bruker's spectrometer software OPUS 7.2. Spectra were acquired within 850–3800 cm⁻¹, utilizing a resolution of 0.5 cm⁻¹ and an aperture of 8 mm. The mirror speed was set to 40 kHz. A Valco Instruments 4/2 valve (Model E2CA, version ED), communicating with the Vertex 70, was employed to rapidly switch between gas flows.

In transient DRIFTS experiments, the gas phase was switched immediately after the background spectrum had been recorded, commencing the measurements. A spectrum was obtained every 5 s and consisted of an average of six individual spectra, each based on five interferograms. One measurement series took 6 min.

3. Results and discussion

3.1. Catalyst characterization and performance

The ceria nanoparticles were first characterized using BET and TEM (for details see Fig. 1 and SI, Figs. S1, and S2). The commercial sample contains particles in the form of polyhedra with a specific surface area of 36 m²/g and a pore volume of 0.08 cm³g⁻¹, whereas the sample

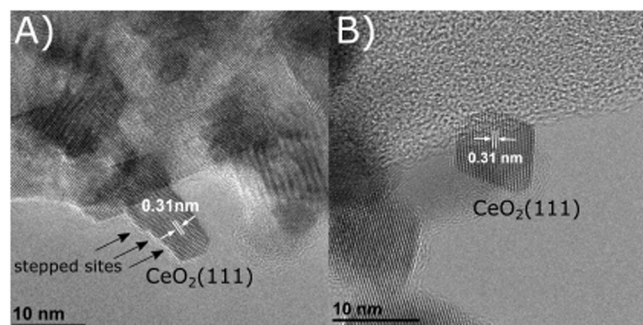


Fig. 1. Detailed TEM images of A) ceria sheets and B) ceria polyhedra. The white arrows indicate the separation of the lattice planes in the direction of the particle surface. Fig. 1A was modified from Ref [14].

prepared by decomposition of cerium nitrate, as described previously [14], contains particles with a sheet shape with a surface area of $57 \text{ m}^2/\text{g}$ and a pore volume of $0.17 \text{ cm}^3/\text{g}^{-1}$. Both samples exhibit a $\text{CeO}_2(111)$ -terminated surface, but the sheets show additional stepped $\text{CeO}_2(111)$ sites (see Fig. 1) [14]. Using ICP-OES, the gold loading was determined as 0.31 wt% for the sheets and 0.27 wt% for the polyhedra. In our previous study on Au/ $\text{CeO}_2(111)$ sheets, the CO-Au vibrations measured by DRIFTS showed a large dispersion of gold due to presence of single atoms and/or smaller clusters, which we assume to be the prepared state also in this study [33]. Contaminations caused by the synthesis, e.g. nitrogen or chlorine, can be excluded within the sensitivity of the XPS measurements.

As summarized in Table 1, both the bare and gold-loaded ceria samples show conversion of CO_2 upon exposure to reaction conditions (4% H_2 , 2% CO_2 , Ar; 100 mL/min) at 250°C . For the unloaded polyhedra and sheets, activities of 2.2% and 1.6% were determined, respectively, while the gold-loaded samples showed significantly higher activities of 5.3% (Au/polyhedra) and 5.4% (Au/sheets). It is noteworthy that the polyhedra yield a higher CO_2 conversion despite their lower surface area. The activity of the gold-loaded samples, on the other hand, does not show a significant difference within the experimental error. In comparison to a previous study on 2.4 wt% Au/ CeO_2 the activity is in the same range ($4.8 \times 10^{-8} \text{ mol}_{\text{CO}}/\text{s}$, 240°C) as reported here [12], while compared to other ceria-based materials [4], our Au/ CeO_2 catalysts show rather high activity considering the low temperature and higher CO_2 concentration. A 2% Pt/ CeO_2 catalyst (Johnson Matthey) has previously been reported to show a conversion of 13.7% at 225°C , but it should be noted that a lower flow rate of 40 mL/min and a $\text{CO}_2:\text{H}_2$ ratio of 1:4 was used, thus preventing a direct comparison of the activity data [34].

3.2. Role of Au and CeO_2

Fig. 2 depicts combined Raman and UV-Vis data of bare and gold-loaded sheets and polyhedra, recorded at 250°C for different gas atmospheres. As discussed below, the Raman F_2g positions and the change in UV-Vis absorption at 550 nm both reflect the reduction of the ceria support. In the following, we will first focus on the F_2g position, which

Table 1

Catalytic activity during rWGS over bare ceria and gold-loaded ceria samples using a feed of $\text{H}_2/\text{CO}_2/\text{Ar}$ (4% H_2 , 2% CO_2 , Ar; 100 mL/min) at 250°C . The catalytic activity was measured after at least 1 h time-on-stream.

Sample	CO_2 conversion	
	%	$\text{mol}_{\text{CO}}/\text{s}$
CeO_2 sheets	1.6	2.2×10^{-8}
CeO_2 polyhedra	2.2	3.0×10^{-8}
0.31 wt% Au/ CeO_2 sheets	5.4	7.3×10^{-8}
0.27 wt% Au/ CeO_2 polyhedra	5.3	7.2×10^{-8}

has previously been shown to be a good indicator for subsurface oxygen defects [14,15,32]. Compared to the starting F_2g positions in argon, it is noticeable that the gold-loaded samples are red-shifted with respect to the unloaded samples, evidencing that the gold-loaded samples possess a larger number of oxygen defects. Based on this observation, one may expect the gold-loaded samples to be more reducible, which is confirmed by changing the gas phase to H_2 . In fact, for the gold-loaded samples a significantly larger redshift than for the unloaded samples is detected, whereby the shift is greatest for the sheets. This behavior demonstrates that polyhedra and sheets are characterized by a different defect formation energy, which is smaller for the sheets. When switching to reaction conditions, all samples show only slight changes, which are within the experimental error, which is why no conclusions should be drawn at this point. However, upon switching to argon, a blueshift is observed, which is indicative of an oxidation of the subsurface and can be explained by a diffusion of oxygen from the bulk to the surface. Such an oxygen diffusion was confirmed by H_2^{18}O experiments in our previous studies on the WGS over Au/ceria catalysts [14,15]. Our results show that reaction intermediates formed during reaction conditions can decompose or desorb in argon, leaving a surface oxygen vacancy and thus promoting an oxygen diffusion from the bulk to the (sub)surface, which results in a F_2g blueshift.

The absorption increase at 550 nm, which can be attributed to a charge transfer from Ce^{3+} to Ce^{4+} [35], allows the change in the oxidation state of the support to be monitored, i.e., the extent of ceria reduction. Comparison of the unloaded and the gold-loaded samples reveals that gold-containing ceria shows a higher absorption at 550 nm already under ex situ conditions (see Fig. 2), which can be explained by the presence of metallic gold giving rise to surface plasmons absorbing in this range [36]. Accordingly, the higher absorption of the gold-loaded polyhedra can be explained by their higher fraction of metallic gold, which is confirmed by the Au 4f photoemissions (see below) and the ex situ UV-Vis spectra (see Fig. S3). Upon heating to 250°C under argon, the gold-loaded samples show an increase in absorption, indicating that the presence of gold can reduce the defect formation energy. When the feed is switched to hydrogen, all samples show an increase, consistent with the Raman results. Interestingly, this reduction-induced increase is also detected for the unloaded polyhedra, but was hardly detected in the Raman F_2g shift, which can be explained by the different information depths of the two methods. Upon exposure to reaction conditions, a slight decrease in absorption can be seen in all samples, resulting from ceria oxidation, whereas switching to argon leads to a more pronounced re-oxidation of the support, in agreement with the Raman results, except for the gold-loaded polyhedra. The UV-Vis behavior of the gold-loaded polyhedra may be explained by the higher fraction of metallic gold and its partial agglomeration during exposure to reducing conditions. Briefly summarizing, all unloaded and gold-loaded samples are subject to gas-phase-dependent oxygen dynamics. A comparison of the extent of ceria reduction, as observed by *operando* Raman and UV-Vis spectroscopy, with the rWGS activity data shows that the role of the support reducibility for the reaction mechanism needs to be further explored.

To gain more detailed insight into the catalysts' vibrational and electronic structure under reductive, reactive, and oxidative conditions, Fig. 3 depicts Raman spectra (left panel) and UV-Vis spectra (right panel) of the gold-loaded samples during exposure to H_2/Ar , reaction conditions, and CO_2/Ar . In the Raman spectra, the band at 243 cm^{-1} , originating from the longitudinal mode of surface oxygen, and the oxygen defect-related band at 550 cm^{-1} are of particular interest [37]. The surface mode shows an increase in intensity during CO_2 exposure, which is more pronounced for the sheets, demonstrating that the surface of the sheets can be re-oxidized more efficiently under CO_2 atmosphere than that of the polyhedra. It is difficult to make statements about the intensity of the defect band as the background changes with the gas atmosphere and thus both re-oxidation and background changes are likely to have an effect on the intensity of the defect band. However, as can be seen from Fig. 3A, the 550 cm^{-1} band is more pronounced for the

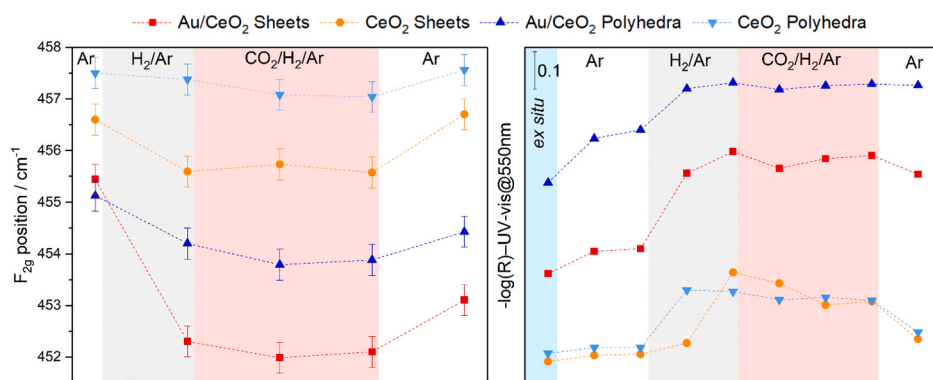


Fig. 2. *In situ* and *operando* Raman (left) and UV-Vis (right) results for Au/CeO₂ sheets and Au/CeO₂ polyhedra together with the corresponding bare support materials recorded during the indicated gas exposures at 250 °C and at a total flow rate of 100 mL/min, except for the *ex situ* spectra, which were taken at 25 °C. The measurement error for the F_{2g} position is indicated. The sample was exposed to each gas phase for about 30 min except for the reaction phase, which was present for 1 h. For details see text.

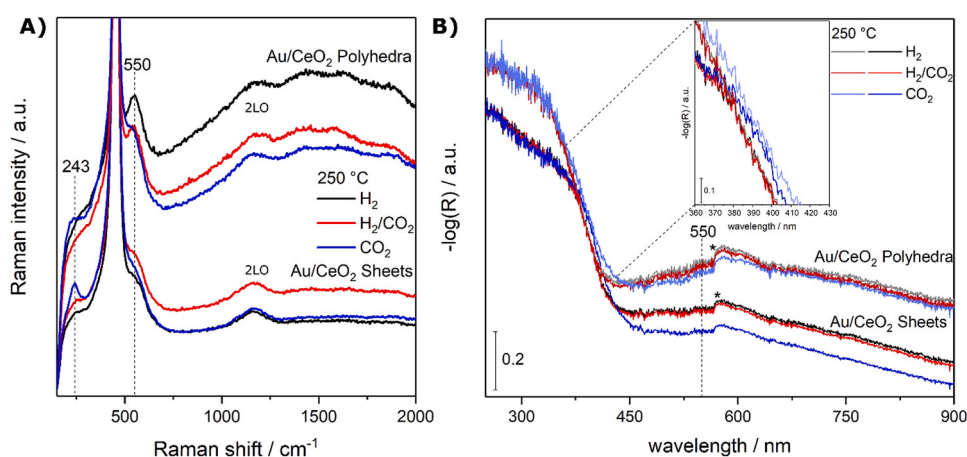


Fig. 3. *Operando* A) Raman and B) UV-Vis spectra of Au/CeO₂ sheets (bottom) and Au/CeO₂ polyhedra (top). The spectra were recorded at 250 °C, at a total flow rate of 100 mL/min, and during gas exposures to H₂ (10%), H₂/CO₂ (4%/2%) and CO₂ (2%). In the Raman spectra the high-intensity F_{2g} peak was cut off to allow an enlarged view of the other features. The inset in the right panel provides an enlarged view of the absorption within 360–430 nm.

polyhedra and its shape changes upon exposure to CO₂. The broad band at 1170 cm⁻¹ is caused by the 2LO overtone [37], whereas additional features above 1250 cm⁻¹ may originate from carbonaceous adsorbates. This aspect will be investigated in more detail using DRIFTS (see below).

The UV-Vis spectra in Fig. 3B show that under CO₂ atmosphere the absorption decreases from about 450 nm on. This effect is more pronounced for the sheets, which can be explained by more facile surface oxidation of the sheets, fully consistent with the intensity increase of the Raman longitudinal surface oxygen mode at 243 cm⁻¹ (see above). The increase in oxidation during exposure to CO₂ also influences the band edge. In fact, as shown in the inset of Fig. 3B, the absorption becomes wider due to the larger band gap, originating from the decrease in Ce³⁺ [35]. Upon switching from H₂ to reaction conditions no significant change in the gold surface plasmon region (~550 nm) was observed, indicating that about the same degree of gold agglomeration is present under both conditions. In this context, it should also be mentioned that previous studies on Au/CeO₂ have shown that H₂ treatment at 200 °C already reduces all cationic gold to metallic gold [38].

Next, the gold-loaded samples were alternately exposed to H₂, CO₂, and reaction conditions, and monitored by combined *operando* Raman and UV-Vis spectroscopy. The results for the F_{2g} position, the absorption at 550 nm, and the gas-phase IR signal are summarized in Fig. 4. The spectroscopic data clearly shows that CO₂ is able to re-oxidize pre-reduced gold-loaded ceria, which can then be reduced again by H₂. The simultaneous gas-phase analysis reveals the formation of H₂O during H₂ treatment, while subsequent treatment with CO₂ leads to CO and H₂O formation (see Fig. 4), demonstrating that hydrogen must still be present on the surface, e.g. as adsorbed water or hydroxide. This observation

will be confirmed by the DRIFTS data (see below). Likewise, after CO₂ treatment followed by exposure to H₂, CO and H₂O are formed (see Fig. 4), which shows the presence of surface carbon species, which only desorb when hydrogen is available. We can rule out residual H₂ or CO₂ as a potential source for the gas-phase signals, as the residence time is about 1 min but the effects continue for more than 10 min. Thus, the results so far would be consistent with a (combined) redox and associative mechanism.

In Fig. 4 it is noticeable that the changes in F_{2g} position and 550 nm absorption are larger for the sheets, underlining their higher redox activity. Interestingly, polyhedra and sheets are characterized by different reduction levels after H₂ treatment (see F_{2g} positions), but show the same F_{2g} position upon exposure to CO₂. This behavior may be an indication that reduced ceria can only be oxidized to a limited extent by using CO₂. Despite equal F_{2g} positions, different absorptions at 550 nm are observed, which can be explained by different fractions of metallic gold clusters.

In the following, we will examine more closely the effect of the pretreatment (H₂ or CO₂) on the reaction process. When the atmosphere is switched from H₂ to reaction conditions, the UV-Vis spectra show a slight decrease in 550 nm absorption and the Raman spectra a small F_{2g} redshift (see Figs. 4 and S4). However, these changes are too small to make a definitive statement. Nevertheless, the situation is different in the case of the CO₂ pretreatment, where the two samples show a pronounced reduction when the reaction conditions are switched on, as indicated by the F_{2g} redshift and the increase in 550 nm absorption, both of which are significantly higher for the sheets. Comparison of the activity data in Figs. 4 and S4 reveals that after pretreatment with CO₂

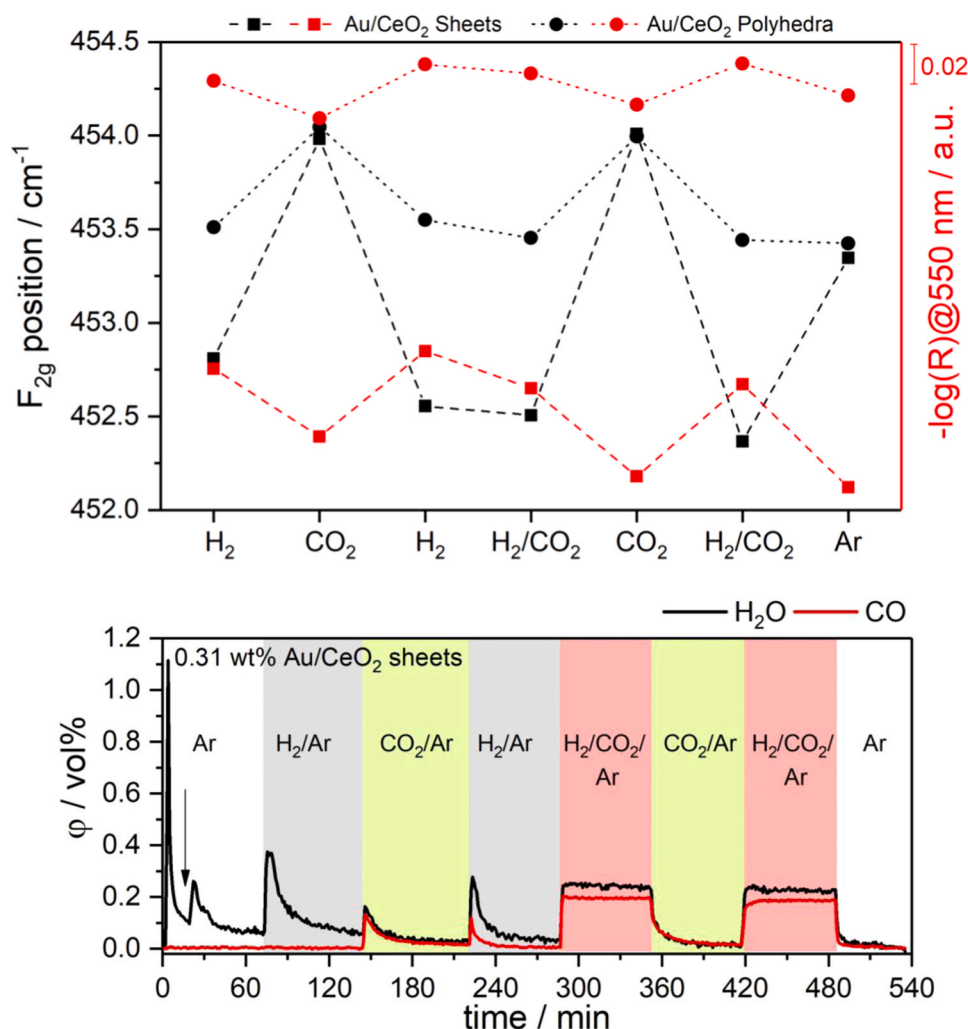


Fig. 4. Top: Operando Raman and UV-Vis results of Au/CeO₂ sheets and Au/CeO₂ polyhedra during exposure to H₂ (10%), CO₂ (2%), H₂/CO₂ (4%/2%), and argon at 250 °C and a total flow rate of 100 mL/min. The data were obtained by averaging two Raman spectra and three UV-Vis spectra per gas phase, except for argon, where the results from only one Raman spectrum and two UV-Vis spectra were used. Bottom: Gas-phase IR analysis of Au/sheets. The corresponding data for Au/polyhedra are shown in Fig. S4. The increased water concentration in the first few minutes is due to the purging of the cell. The cell was heated to 250 °C, starting after 19 min (see black arrow), leading to water desorption and thus an increase in the H₂O concentration.

both samples yield a 0.5% smaller conversion. This behavior suggests that the reaction occurs preferentially over a reduced surface and, as indicated by the F_{2g} shift, lattice oxygen is involved in the reaction mechanism. Another aspect that may affect the activity could be the formation of stable adsorbates during CO₂ treatment, thus blocking active sites. This aspect of the influence of pretreatment will be addressed later in the context of our transient measurements. After reaction conditions, the feed was switched to argon as in the previous measurements (see Fig. 2), which leads to a re-oxidation, whereby the observed changes are significantly larger for the sheets, again showing their increased oxygen mobility.

To investigate the changes in oxidation state of the surface after exposure to different gas atmospheres, *quasi in situ* XPS was applied. In these measurements, XPS spectra were recorded after synthesis, H₂ pretreatment, and reaction conditions without exposure to air when transferring the samples from the pre-treatment/reaction cell to the analysis chamber. It should be mentioned that XPS probes exclusively surface properties, in contrast to Raman and UV-Vis spectroscopy. First of all, XPS analysis did not reveal a significant increase in the surface carbon concentration after reaction conditions (not shown). Hence there is no indication for coking during reaction. As a measure of the surface oxidation state, Table 2 and Fig. S8 depict the O:Ce ratios of the gold-loaded samples, while the corresponding Au 4f photoemissions are shown in Fig. S9. Starting with the O:Ce ratios of the as-prepared samples, both Au/sheets and Au/polyhedra are characterized by approximately the same O:Ce ratio of 1.97. This is indicative of the presence of

Table 2

Surface O:Ce ratios as obtained from the XPS analysis of gold-loaded ceria sheets and polyhedra.

Pretreatment	O:Ce ratio
0.31 wt% Au/CeO ₂ sheets	
None (as prepared)	1.97 ± 0.07
30 min H ₂ (10%), 250 °C	1.83 ± 0.08
1 h H ₂ /CO ₂ (4%/2%), 250 °C	1.75 ± 0.09
0.27 wt% Au/CeO ₂ polyhedra	
None (as prepared)	1.97 ± 0.08
30 min H ₂ (10%), 250 °C	1.50 ± 0.08
1 h H ₂ /CO ₂ (4%/2%), 250 °C	1.39 ± 0.06

surface oxygen defects, and considering that adsorbates such as carbonates or water are still present after synthesis (see outgassing process in Fig. 4), the actual defect content after synthesis will be higher than this value suggests.

Upon treatment with 10% H₂ at 250 °C, a decrease in the O:Ce ratio is observed for both samples, which can readily be explained by a surface reduction due to water formation, as evident from the gas-phase IR measurements (see Fig. 4 and S4). This behavior is also consistent with the F_{2g} redshift and the 550 nm absorption increase discussed above (see Fig. 2). However, upon closer inspection, it can be seen that the stoichiometry change is smaller for the sheets than for the polyhedra, suggesting a lower defect concentration at the surface of the sheets.

At first glance, this observation seems to be in conflict with the Raman and UV-Vis measurements that probe the subsurface. However, the apparent contradiction can be resolved when taking into account the oxygen mobility between surface and subsurface and the fact that oxygen defects are first formed at the surface. In fact, according to the Raman and UV-Vis results, an exchange between surface and subsurface/bulk must have taken place upon switching from reactive to argon atmosphere, because all samples are subject to an F_{2g} blueshift and absorption decrease, despite the inert conditions (see Fig. 4). As these changes are always larger for the sheets, a larger mobility of lattice oxygen in sheets is expected than for the polyhedra. As a consequence of the more facile transfer of oxygen from the subsurface/bulk to the surface, the overall change in the O:Ce surface ratio is smaller for the sheets.

After analysis of the reduction treatment, the sample was transferred to the reaction chamber under absence of air and exposed to reaction conditions, followed by another XPS measurement. As shown in Table 2 and Fig. S8, a further decrease of the O:Ce ratio is detected, but these changes are within the error of the experiment. To this end, we cannot exclude the loss of adsorbates formed under reaction conditions when transferring the sample to the XPS analysis chamber under vacuum conditions. In fact, transient DRIFT spectra clearly show that reaction intermediates desorb immediately after the reaction conditions are stopped by switching off one reactant (see Fig. S6). For these reasons, the quasi *in situ* analysis after reaction conditions needs to be treated with caution.

Next, the state of gold will be addressed based on the Au 4f photoemissions. Due to the low gold loading, a quantitative analysis is challenging (see Fig. S9), but qualitative statements can still be made. Independent of the pretreatment and sample, the state of the gold does not change significantly and metallic or negatively charged gold is present independent of the pretreatment, since the central Au 4f_{7/2} binding energy never exceeds values of 84.5 eV. However, a comparison between polyhedra and sheets shows that the signals of polyhedra are at slightly lower binding energies (~ 0.4 eV), which could indicate more metallic gold, in agreement with the UV-Vis results. In this context, besides the state of gold the presence of potential gold adsorbates should be taken into account. The latter will be addressed by transient DRIFT spectra, as described in the following.

3.3. Transient surface analysis

To gain insight into possible adsorbates during the reaction, transient DRIFT spectra of unloaded and gold-loaded ceria catalysts were recorded, by using spectra of the catalysts under H_2 or CO_2 as background. As the background is measured either in H_2 , CO_2 or H_2/CO_2 , negative signals can occur due to non-stable intermediates. These negative signals are important indicators providing information about the reversibility as well as possible intermediates, which are only formed under reaction conditions. After the background had been recorded, CO_2 or H_2 was added to the constant feed of H_2 or CO_2 , thus switching to reaction conditions, and transient DRIFT spectra were taken every 5 s to monitor the temporal evolution of the adsorbates. By recording the gas-phase composition together with transient DRIFT spectra we confirmed the formation of CO and H_2O under reaction conditions. Fig. 5 depicts transient DRIFT spectra recorded 6 min after switching on the H_2 (A) and CO_2 (B) flow. The same experiments were also performed in reverse, i.e., the catalysts were exposed to reaction conditions and then one reactant was removed (see Fig. S6). Both experiments give comparable results, with the difference that the latter measurements show an inverse trend for the same signals. This reversibility underlines that the corresponding adsorbate bands must be related to reaction intermediates. We also recorded transient DRIFTS after 2 h, largely resembling the behavior after 6 min, and performed modulation excitation (ME) DRIFTS (for details see SI), which show the same bands as our transient DRIFTS experiments, further supporting our claim that the observed bands are associated with reaction intermediates [39].

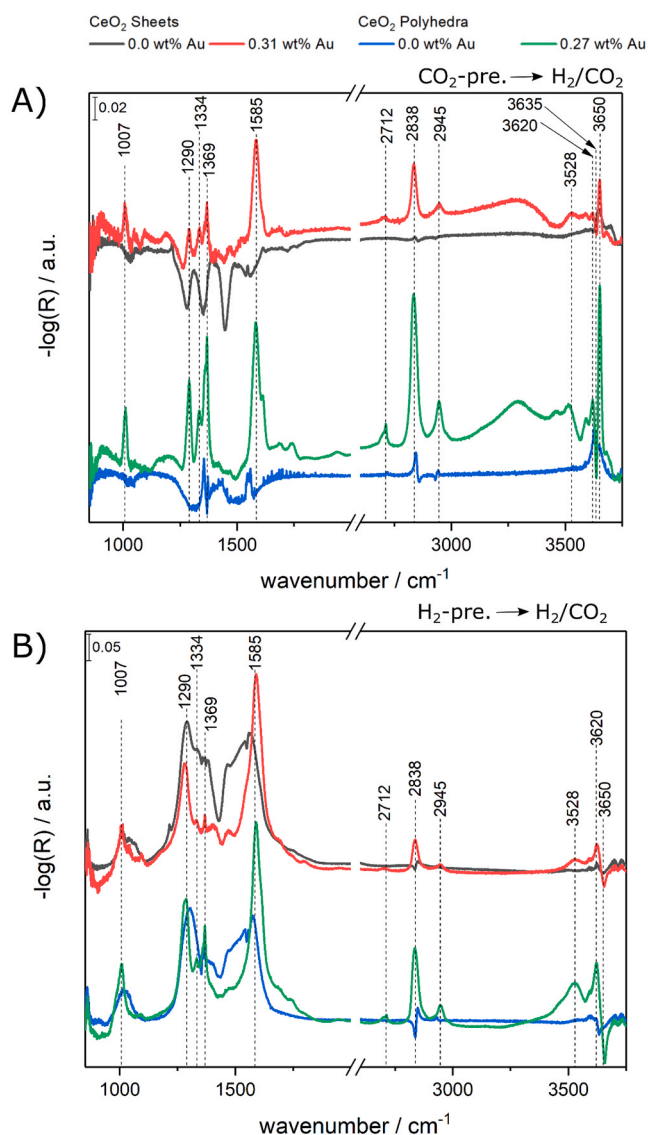


Fig. 5. Transient DRIFT spectra of bare and gold-loaded polyhedra and sheets. The spectra were recorded after pretreatment in H_2 (4 mol%) or CO_2 (2 mol%) balanced in argon at 250 °C at a total gas flow of 100 mL/min. Prior to the measurements **A)** the H_2 supply was switched on while CO_2 remained constant or **B)** the CO_2 supply was switched on while H_2 remained constant. Shown are only the last spectra of a measurement series with a duration of 6 min. As background, spectra of the catalyst after 15-minute exposure to either H_2 (4 mol%) or CO_2 (2 mol%) at 250 °C were employed.

When comparing the sheets and polyhedra in both experiments with and without gold loading, the same overall trends are observed. However, it is noticeable that the signals are sharper for the polyhedra, which contain only one clearly defined surface termination, i.e., $CeO_2(111)$, thus limiting the number of possible adsorbates compared to the sheets which terminate mainly with the $CeO_2(111)$ facet, but exhibit additional steps. Despite the latter differences, the similarities of the adsorbate bands detected for polyhedra and sheet samples point to a dominance of $CeO_2(111)$ -related vibrational features. Therefore, the signals of ceria sheets and polyhedra that can be seen in Fig. 5 will be discussed together in the following.

To trace species related to the reaction, one needs to identify IR bands, which exhibit comparable intensity changes in both experiments, i.e., when either H_2 or CO_2 is switched on. Comparison of the spectra of the gold-loaded sheets and polyhedra in Fig. 5 reveals that this is obviously the case for the C-H stretching signal at 2838 cm^{-1} as well as

its minor neighboring peaks at 2712 cm^{-1} and 2945 cm^{-1} , which are all assigned to bridged/bidentate formate species in agreement with the literature [40–43].

Further confirmation of the presence of formate species may arise from the identification of their complete vibrational pattern, including the region below 2000 cm^{-1} . In this region, signals appear at about 1007 cm^{-1} , 1290 cm^{-1} , 1334 cm^{-1} , 1369 cm^{-1} , and 1585 cm^{-1} in both experiments, which, except for the 1290 cm^{-1} feature, all coincide with the expectations for bridged formate species [40,41]. Regarding bare ceria, formate-related C-H signals can be detected unambiguously for polyhedra only. The identification of other formate bands, identified previously for gold-loaded samples, is hampered by the appearance of negative signals in the carbonate region for the bare samples when switching on H_2 (see Fig. 5A), as will be discussed below. When switching on CO_2 , besides the increasing C-H signal at 2848 cm^{-1} , a nearby negative signal at 2838 cm^{-1} is observed (see Fig. 5B). This indicates that a small part of the formate species may either undergo structural changes or may be subject to changing surroundings, possibly induced by the different redox properties of the reductive gas environment. Therefore, an additional experiment was performed, in which the gas phase was switched between reactive and reducing conditions (see Fig. S5). The observed 10 cm^{-1} redshift of the C-H signal at 2848 cm^{-1} upon reduction is fully consistent with the results in Fig. 5, thus confirming the above hypothesis, while the continuous shift behavior evidences the reversibility of the gas phase-induced changes.

Concerning gold-loaded ceria, the two signals at about 1007 cm^{-1} and 1585 cm^{-1} , together with the intense and characteristic band at 1290 cm^{-1} , suggest the presence of a carbonate species. However, the features at around 1007 cm^{-1} and 1585 cm^{-1} coincide with those of formate (see above). The latter feature furthermore exhibits a shoulder at around 1610 cm^{-1} in both experiments, which may indicate the presence of bidentate carbonates during the reaction. In the literature, bands at around 1610 cm^{-1} have been assigned to hydrogen carbonates or bidentate carbonate, but due to the lack of characteristic hydrogen carbonate bands at 1218 or 1393 cm^{-1} , their presence can be ruled out, thus pointing to the presence of bidentate carbonate [40,41,44].

Fig. 5 shows that for bare ceria the situation is more complex than for gold-loaded samples. When switching on CO_2 (see Fig. 5B), the overall trend of all signals in the carbonate region is positive, as in the case of the gold-loaded samples. In particular, in the region between the two intense bands at about 1290 and 1585 cm^{-1} the signals are broader, indicating the presence of more carbonate species during reaction as compared to gold-loaded ceria. In contrast, when switching from CO_2 atmosphere to reaction conditions (see Fig. 5A), the signals within $1000\text{--}1700\text{ cm}^{-1}$ show a general decrease in intensity, indicating decreased adsorption of CO_2 as carbonates onto the ceria surface. Especially for the sheets, hydrogen carbonates are also present, as evidenced by the characteristic $\delta(\text{OCOH})$ vibration at 1217 cm^{-1} , which is most clearly visible in Figs. 5B and S6B [33].

Important mechanistic conclusions can be drawn from the signal at 1943 cm^{-1} , which is only observed for the gold-loaded samples and increases weakly in both experiments, i.e., after switching on CO_2 and H_2 (see Fig. 6). Fig. 6 provides an enlarged view of the region around 1950 cm^{-1} , together with a spectrum of a Au/sheets sample with $0.62\text{ wt}\%$ gold, i.e., about doubled gold loading, showing an intensity increase of the 1943 cm^{-1} feature with increasing gold loading. The 1943 cm^{-1} feature is attributed to Au-H stretching modes of (partially) dissociatively adsorbed hydrogen, as confirmed by our DFT calculations, in which a hydrogen molecule was placed on a gold atom adsorbed on the (111) surface (see Fig. S17, structure B), corresponding to the most stable $\text{Au}_1/\text{CeO}_2(111)$ structure from our previous studies (see Fig. S17, structure A) [33]. In this case, the calculated H-H distance was 0.93 \AA , compared to a distance of 0.75 \AA for gas-phase H_2 . Based on our experimental observations and DFT results, we propose this state to be stable under reaction conditions only, while in the absence of CO_2 , proton transfer to the nearest oxygen atom takes place, leading to

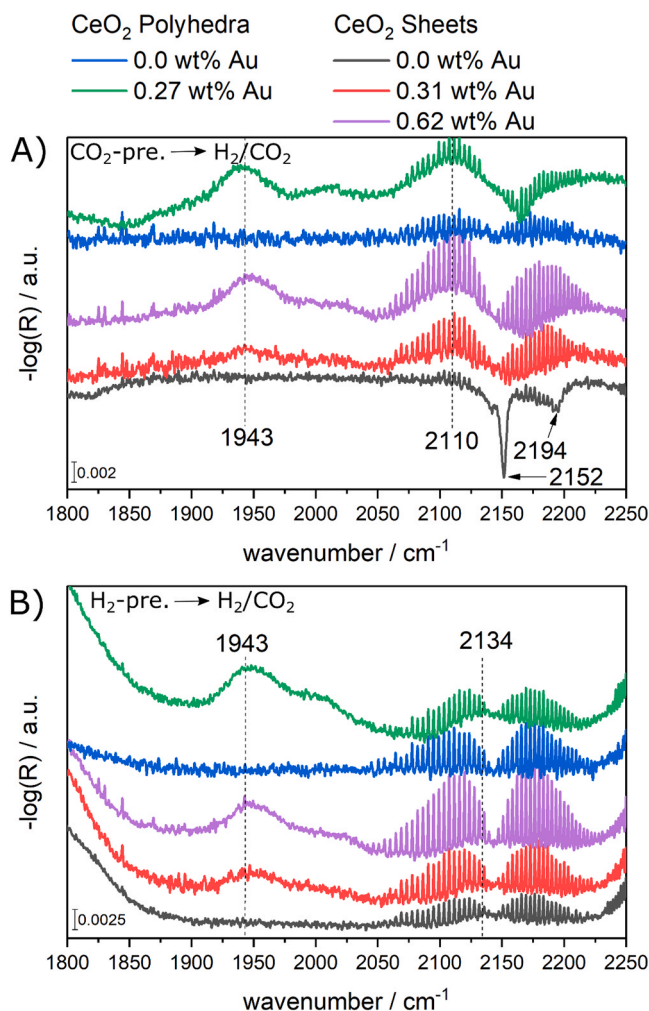


Fig. 6. Enlarged view of *in situ* DRIFT spectra from Fig. 5 showing the presence of adsorbed hydrogen. Spectra were taken A) after the H_2 supply was switched on while CO_2 remained constant, B) after the CO_2 supply was switched on while H_2 remained constant. Shown are only the last spectra of a measurement series with a duration of 6 min. For comparison, spectra of Au/ CeO_2 sheets with $0.62\text{ wt}\%$ gold are shown.

immediate formation of a hydroxide and a Au-H species, since this state is energetically preferred by 1.33 eV (see Fig. S17, structure C). Such a scenario is fully consistent with the absence of the 1943 cm^{-1} band in H_2 atmosphere, i.e., without CO_2 being present (see Fig. S7). In this context, previous studies reported a Au-H species at 2134 cm^{-1} [27]. Remarkably, the 2134 cm^{-1} band is consistent with our DFT calculations and corresponds to a single H atom adsorbed on a gold atom (see Fig. S17, structure C), which is detected here for the gold-loaded sheets and polyhedra, lying underneath the signals of gaseous CO (see Fig. 6). For pretreatment in H_2 atmosphere the Au-H signal has its maximum at exactly 2134 cm^{-1} , whereas in the case of CO_2 pretreatment, the maximum is detected at about 2110 cm^{-1} . This redshift of the maximum may be induced by another signal with negative sign, located at about 2164 cm^{-1} , which may originate from adsorbed CO on $\text{CeO}_2(111)$ [33]. This hypothesis is confirmed by spectra of the bare sheets, which show a contribution from CO adsorbates, as will be discussed below. To the best of our knowledge, we have demonstrated the intermediate step of H_2 adsorption on gold for the first time. It should be mentioned that we also performed isotope exchange experiments. However, the H_2 -Au species is not identifiable by D_2 isotope exchange as the bands shift into the carbonate/formate region and the H_2 -Au region is covered by C-D vibrations of formates (not shown). The theoretical H-D shifts are given in

Table S2.

Based on the DRIFT spectra in Fig. 6, there is no indication for CO adsorbed on gold, since the Au/polyhedra contain larger gold clusters (see above), which would result in IR signals of adsorbed CO below 2100 cm^{-1} [33], and the signals within $2050\text{--}2200\text{ cm}^{-1}$ are less pronounced after pretreatment with H_2 . The latter behavior can be explained by the fact that the signals in this region are assigned to H-Au species (see above), which already exist under the H_2 pretreatment and are thus subtracted by the background. It is noteworthy that the band at 1943 cm^{-1} is asymmetric towards higher wavenumbers, possessing a pronounced shoulder at around 2000 cm^{-1} . We propose this behavior to be caused by the presence of larger gold clusters. To confirm this hypothesis, we placed a hydrogen atom on the most stable $\text{Au}_4/\text{CeO}_2(111)$ structure from our previous DFT studies (see Fig. S17, structure H) [33]. The calculations reveal a characteristic band, which is blue shifted by 23 cm^{-1} compared to our single-site structure. Note that this process is endothermic, with an adsorption energy of 0.31 eV (see Table 2). Thus, this state is not preferred, but it is conceivable that the small energy barrier may be overcome at the elevated temperatures of our experiments and a spillover of hydrogen occurs. Further calculations show that H_2 interacts only weakly with the Au_4 cluster ($E_{\text{ads}} = -0.1\text{ eV}$), in contrast to the single-site adsorption energy of -1.08 eV discussed above (see Table S1). Thus, for larger clusters, no hydrogen dissociation on gold is expected; rather, this band is caused by H atoms from H_2 adsorption on single Au atoms migrating over the ceria surface. This behavior would also be consistent with experiment, as, based on UV-Vis spectra, the polyhedra contain more metallic gold and thus larger gold clusters (see Fig. S3), and these have the most pronounced asymmetry. Regarding the higher 1943 cm^{-1} signal of the polyhedra (despite the presence of larger gold clusters) we point out that, in general, the polyhedra show stronger DRIFTS signals than the sheets (see also Fig. 5). Possible reasons for this behavior may be the larger fraction of single Au atoms in the polyhedra, the higher porosity of the sheets, and/or crystal size/shape effects.

Closer inspection of the transient DRIFT spectra of the bare supports reveals that the sheets exhibit a decreasing feature at 2152 cm^{-1} , which is not detected for the polyhedra (see Fig. 6) and only visible after CO_2 pretreatment and addition of H_2 . The same behavior is also observed for the switching-off experiments (see Fig. S7), i.e., only the bare sheets show an increasing signal at 2152 cm^{-1} after exposure to reaction conditions and after subsequent switching-off of H_2 . This signal is assigned to CO adsorbed on $\text{CeO}_2(111)$, in agreement with the literature [45]. The fact that it is only detected for the ceria sheets suggests that CO adsorbs more strongly at steps than on the flat $\text{CeO}_2(111)$, while exhibiting a similar vibrational frequency. Another interesting observation is that it decreases when H_2 is switched on and increases when H_2 is switched off. Moreover, it remains invisible when CO_2 is switched on after pretreatment in H_2 atmosphere (see Fig. 6). Thus the respective surface species seems to be stable only in the absence of H_2 . Detailed analysis of the spectra in Figs. 5 and 6 reveals that the presence of this CO adsorbate signal correlates with low intensity formate signals in the C-H region at 2838 and 2945 cm^{-1} , in contrast to the ceria polyhedra, which have no adsorbed CO signal and whose formate signals are more intense at the same time. This behavior may indicate that formates are not needed as an intermediate in the rWGS over bare ceria sheets, where stepped sites are present. So, instead of an associative mechanism including formates as intermediates, a redox mechanism involving only surface oxygen atoms may be operative.

Furthermore, at around 2200 cm^{-1} a broad band with increasing intensity is observed for the gold samples in the H_2 -on experiment (see Fig. 6A), which is not present in the CO_2 -on experiment (see Fig. 6B). The same inverse behavior for the intensities is also seen for the switching-off experiments (see Fig. S7). These observations suggest that these species are not involved in the reaction but are spectator species. In previous studies on Zeolite NaY, bands in this region have been attributed to Au^{3+} -CO species [46], and such oxidation states of gold are

also conceivable on $\text{CeO}_2(111)$ if gold occupies a cerium lattice site [47].

Regarding the bare samples, the sheets show a decreasing band at 2194 cm^{-1} , which is detected in the H_2 -on experiment (see Fig. 6A) but not in the switching-off experiments (see Fig. S7), implying that the related species is not involved in the reaction. Due to the decreasing intensity in the H_2 -on and the increasing intensity in the H_2 -off experiment, the band does probably not originate from CO adsorbates, which are formed during the reaction, but probably from weakly adsorbed CO_2 on the reduced surface, which has also been detected in the same range on other oxides such as MgO [48]. Its absence in case of the polyhedra suggests that this process may be influenced by steps.

Based on the transient DRIFTS shown in Fig. 5, OH species are involved in the reaction. For the gold-loaded samples, increasing O-H stretching signals are observed at about 3528 and 3620 cm^{-1} , and the latter show a stronger increase when the CO_2 feed is switched on. The 3620 cm^{-1} band can be assigned to a triply bonded OH group (type III) [49]. Bands at around 3510 cm^{-1} have previously been attributed to a residual oxy-hydroxide phase [50], but our band is sensitive to the different gas environments. Our DFT calculations have revealed that the dissociation of hydrogen on the gold atom leads to a hydroxide species (see above), which is characterized by a vibrational frequency of 3548 cm^{-1} (Fig. S17, structure C). For comparison to the bare support, we have recalculated the most stable hydroxide (H-NNN) from the literature [51] and obtained a vibrational frequency of 3732 cm^{-1} . Based on these findings, we propose the band at 3528 cm^{-1} to originate from hydroxides near gold atoms. Besides, DFT calculations on hydroxides adsorbed on reduced ceria gave significantly higher frequencies than observed here [50].

In contrast, the intense band at about 3650 cm^{-1} increases in intensity upon addition of H_2 (see Fig. 5A), and decreases when CO_2 is switched on (see Fig. 5B). This behavior supports previous assignments of this band to O-H stretching of bridged hydroxide in the presence of an oxygen defect on reduced ceria, which has been referred to as OH (II*-B) [50]. In addition, a feature at about 3635 cm^{-1} rises under oxidizing conditions (see Fig. 5B) and decreases under reducing ones (see Fig. 5A), which is consistent with the corresponding hydroxyl species on unreduced surfaces, i.e., OH (II-B) [50].

Water, the only other final product besides CO, might appear in a gaseous or weakly bound surface state. The spectra of bare ceria exhibit only very weak water-related signals due to rotationally resolved gaseous water between 1400 and 2000 cm^{-1} , as well as above 3500 cm^{-1} . For the gold-loaded catalysts, some gaseous water is visible in Fig. 5A when H_2 is turned on, whereas weakly bound water can be found as a broad increasing signal, centered around 3300 cm^{-1} (see Fig. 5A). Upon addition of CO_2 , no weakly bound water is detected and the rotational bands of gaseous water are by far weaker (see Fig. 5B). The largely missing water signal may be a result of the pretreatment with hydrogen, which leads to the formation of water, that partially desorbs, thus making it invisible in the difference spectra [25].

From the transient DRIFT spectra in Fig. 5 it is apparent that the type of pretreatment has a pronounced influence on the relative intensities of the individual species. In particular, the formate signals gain considerable intensity upon CO_2 pretreatment (see Fig. 5B). On the other hand, the above activity results showed a lower conversion for CO_2 pretreatment than for H_2 pretreatment. Thus, we can already state at this point that the pretreatment has an influence on the reactivity behavior.

4. Discussion of the reaction mechanism

Comparing the degree of reduction obtained by the Raman and UV-Vis analysis with the CO_2 conversions, it is clear that the reducibility of the support does not play the leading role for the rWGS activity. In particular, the polyhedra undergo smaller changes during the different gas exposures than the sheets, but exhibit an activity that is higher for the unloaded sample and about the same for the gold-loaded sample. Therefore, a major question concerns the mechanistic role of gold and

the ceria support in rWGS over Au/ceria catalysts. Our experimental results, especially the transient DRIFT spectra, show that a different mechanism prevails on the gold-loaded samples than on bare ceria. This is supported by the decreasing intensities of bare ceria in the range below 2000 cm^{-1} (see Fig. 5A) and the appearance of additional bands compared to the gold-loaded samples (in this range) when CO_2 is turned on (see Fig. 5B). A redox mechanism alone cannot explain this behavior. We rather propose that an associative mechanism can occur on the polyhedra even in the absence of gold, which is supported by the formate decomposition (see Fig. S6A). Such a behavior is not observed on the sheets. On the other hand, for the sheets, an additional CO-related band is observed at 2152 cm^{-1} , which is not visible for the polyhedra despite the same surface termination, strongly supporting the assumption of a different mechanism on the differently shaped particles. Based on these observations, we propose that on both ceria samples a redox mechanism predominates, but that on the polyhedra also an associative mechanism occurs. In particular, we associate the occurrence of the redox mechanism with the better reducibility of the sheets, originating from the steps. The occurrence of a redox mechanism on both samples is also supported by Fig. S14, which shows an increase of CO in the IR gas phase data when switching from H_2 to CO_2 . At the same time, the switch from CO_2 to H_2 also shows a slight increase in the CO signal for the polyhedra, which is related to the decomposition of remaining carbonaceous adsorbates and thus indicates a reaction pathway via intermediates.

For the gold-loaded samples, an associative mechanism dominates on both samples and is probably facilitated by the easier activation of H_2 in the presence of gold. Nevertheless, on the gold-loaded samples a redox mechanism also takes place, as is apparent from switching between oxidizing and reducing conditions, which evidenced the oxidation or reduction of the surface, leading to CO or H_2O formation (see Fig. 4 and S4). For the rWGS over Au/ TiO_2 catalysts a mechanism involving hydroxycarbonyls has been suggested, which we however exclude for Au/ceria, since we do not detect any CO adsorbed on gold, which is essential for the formation of hydroxycarbonyls. Besides, characteristic carboxylate bands are absent [52], which would indicate the activation of CO_2 on gold. By combining all spectroscopic and theoretical findings of this study, we developed an overall picture of the associative

mechanism on the gold-loaded samples, as summarized in Fig. 7: Starting with a reduced ceria surface (1), the adsorption of CO_2 , facilitated by an oxygen vacancy, leads to carbonate formation (2). Next, carbonate decomposes by release of CO and healing of an oxygen vacancy (3). Reaction of H_2 with surface oxygen results in the formation of water, thereby reducing the surface, while another hydrogen molecule is activated on gold. This activation proceeds in two steps (4). First, a hydrogen molecule dissociatively adsorbs on gold (see Fig. S17, structure B), followed by a spillover onto ceria, forming a hydroxide (see Fig. S17, structure C), as shown by our combination of experiment and theory. Next, a CO_2 molecule adsorbing onto ceria in the vicinity of gold as carbonate (again facilitated by vacancies), is transformed into formate by hydrogen transport from gold to ceria (5). Finally, formate reacts with a neighboring hydroxide, leading to water and CO formation, thus closing the catalytic cycle. The individual reaction steps are summarized in Fig. S16.

We point out that there are two routes by which CO_2 can be activated, i.e., via carbonates or formates/hydroxycarbonyls [53,54]. Theoretical studies [53] indicate that the route via hydroxycarbonyls (COOH) is more competitive than that via formates (HCOO), but based on the absence of specific hydroxycarbonyls bands [55] in our IR experiments, the route via COOH appears to play a minor role. Furthermore, H_2 pretreatment leads to a reduced surface and supports the dissociation of CO_2 to CO via carbonates [53], which is consistent with our observation of higher activities after H_2 pretreatment and the lower C-H signals in Fig. 5B. This step is also proposed to be rate-determining, since the healing of defects by CO_2 via the release of CO ($\text{CeO}_2(111)$ without gold) is endothermic by 0.98 eV. Based on our findings, the formate and carbonate formation steps (5, 2) cannot be explicitly separated from each other, thus these steps may run independently of each other. For example, by omitting steps 2 and 3, the reaction may proceed directly to step 4. This is also consistent with the higher C-H intensities in the measurements with CO_2 pretreatment (see Fig. 5A), which are starting from a more oxidized surface compared to the H_2 pretreatment. Studies during methane dry reforming over ^{18}O labeled Ni/ CeO_2 have shown, that lattice oxygen is involved in the formation of CO [56]. However, in the reaction discussed here, no coking of the catalyst can be detected, so the involvement of lattice oxygen in CO

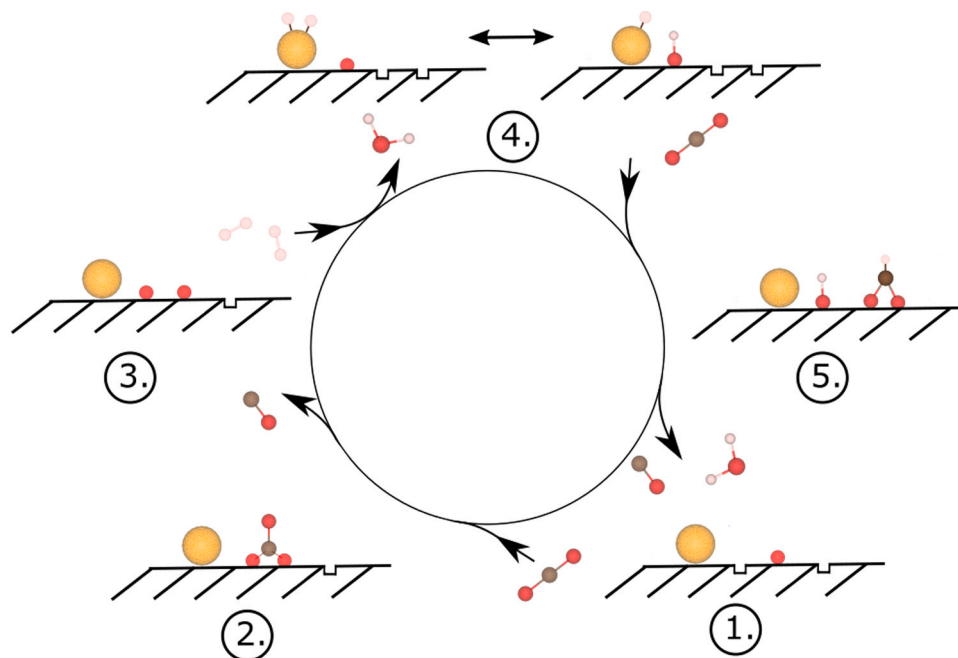


Fig. 7. Proposed mechanism for the reverse water-gas shift reaction (rWGS) over Au/ $\text{CeO}_2(111)$ catalysts. For clarity, only the reaction pathway mediated by a gold single site is shown. Atoms correspond to oxygen (red), carbon (brown), hydrogen (white) and gold (gold).

formation similar to methane dry reforming is improbable. Nevertheless, such studies could support the involvement of lattice oxygen in the formation of H₂O. In summary, the CO₂ reduction pathway depends on the concentration of defects and/or hydroxides, which in turn depend on the pretreatment (see also Fig. S13). Thus, on a defect-rich surface (H₂ pretreatment), the path via carbonates is preferred, while on the other hand, on a surface with fewer defects, the path via formates will dominate.

5. Conclusions

Based on the *operando* Raman and UV-Vis spectroscopic observations, the ability to form defects plays a minor role in the conversion of CO₂ within the rWGS. Indeed, when the reducibility of the gold-loaded samples is compared, sheets undergo significantly larger changes under reducing (H₂) or reaction conditions (see Fig. 3), while their activity is very similar to that of the polyhedra (see Table 1). These observations are evidence of the fact that defect formation is not essential for the reaction pathway and that the route via intermediates (formates, carbonates, hydroxides) is more important. However, detailed analysis reveals that the pretreatment (H₂, CO₂) has an influence on the reaction pathway and on the catalytic activity. To this end, CO₂ reduction over a reduced ceria surface favors carbonate intermediates, while over a low-defect surface a reduction via formates is preferred; besides, starting from a highly reduced surface (H₂ pretreatment) leads to higher activities.

In contrast to bare ceria, a pure redox mechanism loses importance on Au/ceria catalysts at lower temperatures (<250 °C). This is attributed to the activation of hydrogen on gold atoms, whereas hydrogen interacts in its molecular form only very weakly with the bare CeO₂(111) surface [51]. In this context, using transient DRIFTS in combination with DFT calculations, we were able to elucidate for the first time the individual steps of H₂ activation over Au/CeO₂(111), which is shown to proceed in two steps (see Fig. 7). Based on our findings, we propose gold atoms to be essential for an associative mechanism.

Our study clearly reveals that multiple techniques, sampling both subsurface and surface properties, are required to elucidate the mechanism of the rWGS over Au/CeO₂ catalysts. In particular, the use of *operando* and transient approaches in combination with theory is shown to enable a detailed analysis, including spectroscopic features not reported in the literature.

CRediT authorship contribution statement

Marc Ziemba, Jakob Weyel: Investigation, Methodology, Software, Validation, Formal analysis, Data curation, Visualization, Writing – original draft. **Christian Hess:** Conceptualization, Visualization, Supervision, Project Administration, Funding acquisition, Writing – review & editing.

Declaration of Competing Interest

The authors declare that they have no known competing financial interests or personal relationships that could have appeared to influence the work reported in this paper.

Acknowledgement

We thank Stefan Lauterbach and Hans-Joachim Kleebe for TEM measurements, Martin Brodrecht for BET measurements, M. Verónica Ganduglia-Pirovano for support in theory, and Karl Kopp for technical support and helpful discussions on the XPS results. Calculations for this research were conducted on the Lichtenberg high performance computer of the TU Darmstadt. Jakob Weyel gratefully acknowledges a scholarship from the Fonds der Chemischen Industrie im Verband der

Chemischen Industrie e.V.

Appendix A. Supporting information

Supplementary data associated with this article can be found in the online version at doi:10.1016/j.apcatb.2021.120825.

References

- [1] J. Jiang, B. Ye, J. Liu, Research on the peak of CO₂ emissions in the developing world: current progress and future prospect, Appl. Energy 235 (2019) 186–203, <https://doi.org/10.1016/j.apenergy.2018.10.089>.
- [2] X. Chen, Y. Chen, C. Song, P. Ji, N. Wang, W. Wang, L. Cui, Recent advances in supported metal catalysts and oxide catalysts for the reverse water-gas shift reaction, Front. Chem. 8 (2020) 1–21, <https://doi.org/10.3389/fchem.2020.00709>.
- [3] M. Boaro, S. Colussi, A. Trovarelli, Ceria-based materials in hydrogenation and reforming reactions for CO₂ valorization, Front. Chem. 7 (2019) 28, <https://doi.org/10.3389/fchem.2019.00028>.
- [4] K. Chang, H. Zhang, M. Cheng, Q. Lu, Application of ceria in CO₂ conversion catalysis, ACS Catal. 10 (2020) 613–631, <https://doi.org/10.1021/acscatal.9b03935>.
- [5] G. Jacobs, B.H. Davis, Reverse water-gas shift reaction: steady state isotope switching study of the reverse water-gas shift reaction using in situ DRIFTS and a Pt/ceria catalyst, Appl. Catal. A Gen. 284 (2005) 31–38, <https://doi.org/10.1016/j.apcata.2005.01.013>.
- [6] F.C. Meunier, D. Tibiletti, A. Goguet, D. Reid, R. Burch, On the reactivity of carbonate species on a Pt/CeO₂ catalyst under various reaction atmospheres: Application of the isotopic exchange technique, Appl. Catal. A Gen. 289 (2005) 104–112, <https://doi.org/10.1016/j.apcata.2005.04.018>.
- [7] C.M. Kalamaras, S. Americanou, A.M. Efstathiou, “Redox” vs “associative formate with –OH group regeneration” WGS reaction mechanism on Pt/CeO₂: Effect of platinum particle size, J. Catal. 279 (2011) 287–300, <https://doi.org/10.1016/j.jcat.2011.01.024>.
- [8] L. Lin, S. Yao, Z. Liu, F. Zhang, N. Li, D. Vovchok, A. Martínez-Arias, R. Castañeda, J. Lin, S.D. Senanayake, D. Su, D. Ma, J.A. Rodriguez, In situ characterization of Cu/CeO₂ nanocatalysts for CO₂ hydrogenation: morphological effects of nanostructured ceria on the catalytic activity, J. Phys. Chem. C. 122 (2018) 12934–12943, <https://doi.org/10.1021/acs.jpcc.8b03596>.
- [9] Y. Liu, Z. Li, H. Xu, Y. Han, Reverse water-gas shift reaction over ceria nanocube synthesized by hydrothermal method, Catal. Commun. 76 (2016) 1–6, <https://doi.org/10.1016/j.cattcom.2015.12.011>.
- [10] L.F. Bobadilla, J.L. Santos, S. Ivanova, J.A. Odriozola, A. Urakawa, Unravelling the role of oxygen vacancies in the mechanism of the reverse water–gas shift reaction by *operando* DRIFTS and ultraviolet–visible spectroscopy, ACS Catal. 8 (2018) 7455–7467, <https://doi.org/10.1021/acscatal.8b02121>.
- [11] J.A. Rodríguez, J. Evans, J. Graciani, J.-B. Park, P. Liu, J. Hrbek, J.F. Sanz, High water–gas shift activity in TiO₂(110) supported Cu and Au nanoparticles: role of the oxide and metal particle size, J. Phys. Chem. C. 113 (2009) 7364–7370, <https://doi.org/10.1021/jp900483u>.
- [12] L.C. Wang, M. Tahvildar Khazaneh, D. Widmann, R.J. Behm, TAP reactor studies of the oxidizing capability of CO₂ on a Au/CeO₂ catalyst – a first step toward identifying a redox mechanism in the reverse water–gas shift reaction, J. Catal. 302 (2013) 20–30, <https://doi.org/10.1016/j.jcat.2013.02.021>.
- [13] L.C. Wang, D. Widmann, R.J. Behm, Reactive removal of surface oxygen by H₂, CO and CO/H₂ on a Au/CeO₂ catalyst and its relevance to the preferential CO oxidation (PROX) and reverse water gas shift (RWGS) reaction, Catal. Sci. Technol. 5 (2015) 925–941, <https://doi.org/10.1039/C4CY01030B>.
- [14] C. Schilling, C. Hess, Elucidating the role of support oxygen in the water–gas shift reaction over ceria-supported gold catalysts using *operando* spectroscopy, ACS Catal. 9 (2019) 1159–1171, <https://doi.org/10.1021/acscatal.8b04536>.
- [15] M. Ziemba, M.V. Ganduglia-Pirovano, C. Hess, Insight into the mechanism of the water–gas shift reaction over Au/CeO₂ catalysts using combined *operando* spectroscopies, Faraday Discuss. 229 (2021) 232–250, <https://doi.org/10.1039/C9FD00133F>.
- [16] X. Fu, L. Guo, W. Wang, C. Ma, C. Jia, K. Wu, R. Si, L.-D. Sun, C.-H. Yan, Direct identification of active surface species for the water–gas shift reaction on a gold–ceria catalyst, J. Am. Chem. Soc. 141 (2019) 4613–4623, <https://doi.org/10.1021/jacs.8b09306>.
- [17] A.M. Efstathiou, Catalysis, Royal Society of Chemistry, Cambridge, 2016, <https://doi.org/10.1039/9781782626855>.
- [18] T. Staudt, Y. Lykhach, N. Tsud, T. Skála, K.C. Prince, V. Matolín, J. Libuda, Ceria reoxidation by CO₂: a model study, J. Catal. 275 (2010) 181–185, <https://doi.org/10.1016/j.jcat.2010.07.032>.
- [19] S. Ackermann, L. Sauvin, R. Castiglioni, J.L.M. Rupp, J.R. Scheffe, A. Steinfeld, Kinetics of CO₂ reduction over nonstoichiometric ceria, J. Phys. Chem. C. 119 (2015) 16452–16461, <https://doi.org/10.1021/acs.jpcc.5b03464>.
- [20] J.A. Rodríguez, D.C. Grinter, Z. Liu, R.M. Palomino, S.D. Senanayake, Ceria-based model catalysts: fundamental studies on the importance of the metal–ceria interface in CO oxidation, the water–gas shift, CO₂ hydrogenation, and methane and alcohol reforming, Chem. Soc. Rev. 46 (2017) 1824–1841, <https://doi.org/10.1039/c6cs00863a>.

- [21] J.H. Carter, G.J. Hutchings, Recent advances in the gold-catalysed low-temperature water–gas shift reaction, *Catalysts* 8 (2018) 627, <https://doi.org/10.3390/catal8120627>.
- [22] A.M. Abdel-Mageed, G. Kučerová, J. Bansmann, R.J. Behm, Active Au species during the low-temperature water gas shift reaction on Au/CeO₂: a time-resolved operando XAS and DRIFTS study, *ACS Catal.* 7 (2017) 6471–6484, <https://doi.org/10.1021/acscatal.7b01563>.
- [23] J.H. Carter, X. Liu, Q. He, S. Althahban, E. Nowicka, S.J. Freakley, L. Niu, D. J. Morgan, Y. Li, J.W.H. Niemantsverdriet, S. Golunski, C.J. Kiely, G.J. Hutchings, Activation and deactivation of gold/ceria-zirconia in the low-temperature water-gas shift reaction, *Angew. Chem. Int. Ed.* 56 (2017) 16037–16041, <https://doi.org/10.1002/anie.201709708>.
- [24] (a) A.M. Efstathiou, K.C. Petalidou, Reply to the Letter to the Editor concerning the comments of Dr. F. Meunier to the article, *Appl. Catal. B: Environ.* 136–137 (2013) 225–238; (b) Kalamaras, et al., titled “The effect of La³⁺-doping of CeO₂ support on the water–gas shift re, *Appl. Catal. B Environ.* 152–153 (2014) 439–443, <https://doi.org/10.1016/j.apcatb.2014.01.064>.
- [25] D. Schweke, L. Shelly, R. Ben David, A. Danon, N. Kostirya, S. Hayun, Comprehensive study of the ceria–H₂ system: effect of the reaction conditions on the reduction extent and intermediates, *J. Phys. Chem. C* 124 (2020) 6180–6187, <https://doi.org/10.1021/acs.jpcc.9b11975>.
- [26] Z. Wu, Y. Cheng, F. Tao, L. Daemen, G.S. Foo, L. Nguyen, X. Zhang, A. Beste, A. J. Ramirez-Cuesta, Direct neutron spectroscopy observation of cerium hydride species on a cerium oxide catalyst, *J. Am. Chem. Soc.* 139 (2017) 9721–9727, <https://doi.org/10.1021/jacs.7b05492>.
- [27] R. Juárez, S.F. Parker, P. Concepción, A. Corma, H. García, Heterolytic and heterotopic dissociation of hydrogen on ceria-supported gold nanoparticles. Combined inelastic neutron scattering and FT-IR spectroscopic study on the nature and reactivity of surface hydrogen species, *Chem. Sci.* 1 (2010) 731, <https://doi.org/10.1039/c0sc00336k>.
- [28] D. Ren, L. He, L. Yu, R.-S. Ding, Y.-M. Liu, Y. Cao, H.-Y. He, K.-N. Fan, An unusual chemoselective hydrogenation of quinoline compounds using supported gold catalysts, *J. Am. Chem. Soc.* 134 (2012) 17592–17598, <https://doi.org/10.1021/ja3066978>.
- [29] H.Y. Kim, G. Henkelman, CO Oxidation at the interface of Au nanoclusters and the stepped-CeO₂(111) surface by the Mars–van Krevelen mechanism, *J. Phys. Chem. Lett.* 4 (2013) 216–221, <https://doi.org/10.1021/jz301778b>.
- [30] C. Schilling, C. Hess, CO Oxidation on ceria supported gold catalysts studied by combined operando Raman/UV–Vis and IR spectroscopy, *Top. Catal.* 60 (2017) 131–140, <https://doi.org/10.1007/s11244-016-0732-6>.
- [31] C. Schilling, M.V. Ganduglia-Pirovano, C. Hess, Experimental and theoretical study on the nature of adsorbed oxygen species on shaped ceria nanoparticles, *J. Phys. Chem. Lett.* 9 (2018) 6593–6598, <https://doi.org/10.1021/acs.jpclett.8b02728>.
- [32] M. Ziemba, C. Hess, Influence of gold on the reactivity behaviour of ceria nanorods in CO oxidation: combining operando spectroscopies and DFT calculations, *Catal. Sci. Technol.* 10 (2020) 3720–3730, <https://doi.org/10.1039/D0CY00392A>.
- [33] C. Schilling, M. Ziemba, C. Hess, M.V. Ganduglia-Pirovano, Identification of single-atom active sites in CO oxidation over oxide-supported Au catalysts, *J. Catal.* 383 (2020) 264–272, <https://doi.org/10.1016/j.jcat.2020.01.022>.
- [34] A. Goguet, F.C. Meunier, D. Tibiletti, J.P. Breen, R. Burch, Spectrokinetic investigation of reverse water-gas-shift reaction intermediates over a Pt/CeO₂ catalyst, *J. Phys. Chem. B* 108 (2004) 20240–20246, <https://doi.org/10.1021/jp047242w>.
- [35] C.W.M. Castleton, J. Kullgren, K. Hermansson, Tuning LDA+U for electron localization and structure at oxygen vacancies in ceria, *J. Chem. Phys.* 127 (2007), 244704, <https://doi.org/10.1063/1.2800015>.
- [36] J.A. Hernández, S.A. Gómez, T.A. Zepeda, J.C. Fierro-González, G.A. Fuentes, Insight into the deactivation of Au/CeO₂ catalysts studied by in situ spectroscopy during the CO-PROX reaction, *ACS Catal.* 5 (2015) 4003–4012, <https://doi.org/10.1021/acscatal.5b00739>.
- [37] C. Schilling, A. Hofmann, C. Hess, M.V. Ganduglia-Pirovano, Raman spectra of polycrystalline CeO₂: a density functional theory study, *J. Phys. Chem. C* 121 (2017) 20834–20849, <https://doi.org/10.1021/acs.jpcc.7b06643>.
- [38] A.M. Abdel-Mageed, G. Kučerová, J. Bansmann, R.J. Behm, Active Au species during the low-temperature water gas shift reaction on Au/CeO₂: a time-resolved operando XAS and DRIFTS study, *ACS Catal.* 7 (2017) 6471–6484, <https://doi.org/10.1021/acscatal.7b01563>.
- [39] V. Marchionni, D. Ferri, O. Kröcher, A. Wokaun, Increasing the sensitivity to short-lived species in a modulated excitation experiment, *Anal. Chem.* 89 (2017) 5801–5809, <https://doi.org/10.1021/acs.analchem.6b04939>.
- [40] G.N. Vayssilov, M. Mihaylov, P.S. Petkov, K.I. Hadjiivanov, K.M. Neyman, Reassignment of the vibrational spectra of carbonates, formates, and related surface species on ceria: a combined density functional and infrared spectroscopy investigation, *J. Phys. Chem. C* 115 (2011) 23435–23454, <https://doi.org/10.1021/jp208050a>.
- [41] F. Romero-Sarria, L.M. Martínez, T.M.A. Centeno, J.A. Odriozola, Surface dynamics of Au/CeO₂ catalysts during CO oxidation, *J. Phys. Chem. C* 111 (2007) 14469–14475, <https://doi.org/10.1021/jp073541k>.
- [42] D. Vovchok, C. Zhang, S. Hwang, L. Jiao, F. Zhang, Z. Liu, S.D. Senanayake, J. A. Rodriguez, Deciphering dynamic structural and mechanistic complexity in Cu/CeO₂/ZSM-5 catalysts for the reverse water-gas shift reaction, *ACS Catal.* 10 (2020) 10216–10228, <https://doi.org/10.1021/acscatal.0c01584>.
- [43] W.O. Gordon, Y. Xu, D.R. Mullins, S.H. Overbury, Temperature evolution of structure and bonding of formic acid and formate on fully oxidized and highly reduced CeO₂(111), *Phys. Chem. Chem. Phys.* 11 (2009) 11171–11183, <https://doi.org/10.1039/b913310k>.
- [44] Y. Denkwitz, A. Karpenko, V. Plzak, R. Leppelt, B. Schumacher, R.J. Behm, Influence of CO₂ and H₂ on the low-temperature water–gas shift reaction on Au/CeO₂ catalysts in idealized and realistic reformate, *J. Catal.* 246 (2007) 74–90, <https://doi.org/10.1016/j.jcat.2006.11.012>.
- [45] C. Wöll, Structure and chemical properties of oxide nanoparticles determined by surface-ligand IR spectroscopy, *ACS Catal.* (2019), <https://doi.org/10.1021/acscatal.9b04016>.
- [46] M.Y. Mihaylov, J.C. Fierro-Gonzalez, H. Knözinger, B.C. Gates, K.I. Hadjiivanov, Formation of nonclassical carbonyls of Au³⁺ in zeolite NaY: characterization by infrared spectroscopy, *J. Phys. Chem. B* 110 (2006) 7695–7701, <https://doi.org/10.1021/jp057426q>.
- [47] M.F. Camellone, S. Fabris, Reaction mechanisms for the CO oxidation on Au/CeO₂ catalysts: activity of substitutional Au³⁺/Au⁺ cations and deactivation of supported Au⁺ adatoms, *J. Am. Chem. Soc.* 131 (2009) 10473–10483, <https://doi.org/10.1021/ja902109k>.
- [48] I.M. Hill, S. Hanspal, Z.D. Young, R.J. Davis, DRIFTS of Probe molecules adsorbed on magnesia, zirconia, and hydroxyapatite catalysts, *J. Phys. Chem. C* 119 (2015) 9186–9197, <https://doi.org/10.1021/jp509889j>.
- [49] A. Laachir, V. Perrichon, A. Badri, J. Lamotte, E. Catherine, J.C. Lavalley, J. El Fallah, L. Hilaire, F. Le Normand, E. Quéméré, G.N. Sauvion, O. Touret, Reduction of CeO₂ by hydrogen. Magnetic susceptibility and Fourier-transform infrared, ultraviolet and X-ray photoelectron spectroscopy measurements, *J. Chem. Soc. Faraday Trans. 87* (1991) 1601–1609, <https://doi.org/10.1039/FT9918701601>.
- [50] A. Badri, C. Binet, J. Lavalley, An FTIR study of surface ceria hydroxy groups during a redox process with H₂, *J. Chem. Soc. Faraday Trans.* 92 (1996) 4669, <https://doi.org/10.1039/ft9969204669>.
- [51] D. Fernández-Torre, J. Carrasco, M.V. Ganduglia-Pirovano, R. Pérez, Hydrogen activation, diffusion, and clustering on CeO₂(111): A DFT+U study, *J. Chem. Phys.* 141 (2014), 014703, <https://doi.org/10.1063/1.4885546>.
- [52] E.T. Saw, U. Oemar, M.L. Ang, H. Kus, S. Kawi, High-temperature water gas shift reaction on Ni–Cu/CeO₂ catalysts: effect of ceria nanocrystal size on carboxylate formation, *Catal. Sci. Technol.* 6 (2016) 5336–5349, <https://doi.org/10.1039/C5CY01932J>.
- [53] X. Lu, W. Wang, S. Wei, C. Guo, Y. Shao, M. Zhang, Z. Deng, H. Zhu, W. Guo, Initial reduction of CO₂ on perfect and O-defective CeO₂(111) surfaces: towards CO or COOH? *RSC Adv.* 5 (2015) 97528–97535, <https://doi.org/10.1039/c5ra17825h>.
- [54] Y. Yang, S. Wang, Y. Jiang, X. Wu, C. Xia, R. Peng, Y. Lu, CO₂ Activation and reduction on Pt–CeO₂-based catalysts, *J. Phys. Chem. C* 123 (2019) 17092–17101, <https://doi.org/10.1021/acs.jpcc.9b02878>.
- [55] O. Pozdnyakova, D. Teschner, A. Wootsch, J. Krohnert, B. Steinhauer, H. Sauer, L. Toth, F. Jentoft, A. Knopgericke, A. Knopgericke, Z. Paal, Preferential CO oxidation in hydrogen (PROX) on ceria-supported catalysts, part I: oxidation state and surface species on Pt/CeO₂ under reaction conditions, *J. Catal.* 237 (2006) 1–16, <https://doi.org/10.1016/j.jcat.2005.10.014>.
- [56] C.M. Damaskinos, J. Zavašnik, P. Djinović, A.M. Efstathiou, Dry reforming of methane over Ni/Ce_{0.8}Ti_{0.2}O_{2-δ}: the effect of Ni particle size on the carbon pathways studied by transient and isotopic techniques, *Appl. Catal. B Environ.* 296 (2021), 120321, <https://doi.org/10.1016/j.apcatb.2021.120321>.